

Ultrathin chromia films grown with preferential texture on metallic, semimetallic and insulating substrates



Xumin Chen ^a, Haseeb Kazi ^b, Yuan Cao ^c, Bin Dong ^c, Frank L. Pasquale ^c, Juan A. Colón Santana ^d, Shi Cao ^a, Michael Street ^a, Raymond Welch ^c, Ch Binek ^a, Axel Enders ^a, Jeffrey A. Kelber ^c, P.A. Dowben ^{a,*}

^a Department of Physics and Astronomy, University of Nebraska, Theodore Jorgensen Hall, 855 North 16th Street, PO Box 880299, Lincoln, NE 68588-0299, USA

^b Department of Materials Science and Engineering, University of North Texas, 1155 Union Circle, #305070, Denton, TX 76203-5017, USA

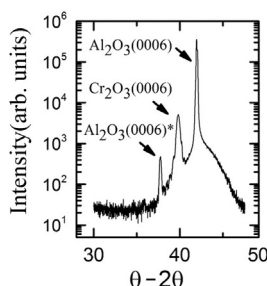
^c Department of Chemistry, University of North Texas, 1155 Union Circle, #305070, Denton, TX 76203-5017, USA

^d Nebraska Center for Energy Sciences Research, 230 Whittier, 2200 Vine Street, Lincoln, NE 68583-0857, USA

HIGHLIGHTS

- Ultra thin film growth of chromia, Cr₂O₃, possible.
- Evidence for strong texture growth of chromia, regardless of substrate.
- Lattice match not necessary for texture growth of chromia.
- Chromia growth on graphitic carbon possible.
- While chromium does not ‘wet’ Cu(111), but chromia does.

GRAPHICAL ABSTRACT



ARTICLE INFO

Article history:

Received 5 February 2014

Received in revised form

22 September 2014

Accepted 29 September 2014

Available online 7 October 2014

Keywords:

Oxides

Thin films

Low energy electron diffraction (LEED)

Magnetic materials

Vacuum deposition

X-ray photoelectron spectroscopy

ABSTRACT

The growth and surface structures of ultrathin chromia (Cr₂O₃) films on Cu(111), Co(0001), and on thin graphene/graphitic carbon films on Co(0001) have been investigated, and compared to epitaxial chromia films grown on Al₂O₃(0001). On metallic substrates, chromia grows with strong texture along the (0001) direction with little mosaic spread. On cobalt, a thin interfacial oxide is observed, which is stable upon exposure to ambient or annealing in ultrahigh vacuum. In the case of chromia growth on graphite, chromia-catalyzed oxidation and etching of the carbon layers is observed above 800 K in ultra high vacuum. The results show that highly ordered and continuous, ultrathin films of chromia (Cr₂O₃) can be grown on a variety of substrates and that magnetic tunnel junction structures, based on the magneto-electric chromium oxide, may be built from the “bottom up”.

© 2014 Elsevier B.V. All rights reserved.

1. Introduction

Recently, Cr₂O₃ has attracted considerable attention as a magneto-electric with roughness-insensitive boundary spin polarization [1–5]. This boundary magnetization is key to the recent demonstration of robust isothermal electric control of exchange

* Corresponding author.

E-mail addresses: pdowben@unl.edu, pdowben1@unl.edu (P.A. Dowben).

bias at room temperature [1]. Magneto-electrics are a possible route for voltage control of magnetization in a magnetic tunnel junction structure [4,6,7] or as a magneto-electric dielectric gate to a spin field effect transistor [8–11]. The implementation of a magneto-electric like chromia would benefit from the facile ultra-thin film growth of chromia on both ferromagnetic and paramagnetic electrode materials, like cobalt and copper. The barriers to magneto-electric switching are thought to scale roughly with volume, so thinner films might facilitate this voltage controlled switching of the interface polarization. Of course this also requires that the magneto-electric properties are retained in the thin film limit at elevated temperatures, but if this is indeed the case then the material may require a smaller critical voltage, and possibly exhibit higher switching speeds as well. There is experimental evidence that in fact this is correct [12]. Unfortunately there is a limit to preserving useful magneto-electric properties, as in the thin film limit the boundary magnetization dominates. We have shown that for ultra-thin chromia films close to the Néel temperature, a magnetic field alone can switch the entire antiferromagnetic spin structure through Zeemann coupling with the boundary magnetization [12]. The growth of thin epitaxial films on magnetic and non-magnetic substrates is therefore a necessary first step towards the study of the film morphology and interfacial chemistry, including interface oxidation and charge transfer, and how they affect chromia magnetoelectric properties in the thin film limit. There is an unexplored regime of film thickness, below which chromia thin films cannot be used to switch the magnetization of an adjacent ferromagnet. Likely only chromia films above some critical thickness will be effective for exchange bias applications, even without electric/voltage controlled switching.

There has been a long standing interest in chromia, which also extends to possible applications as a catalyst or photo-catalyst [13–37], leading to a very rich literature of the interface properties of this material. There have been a number of studies of successful chromia thin film growth on a variety of substrates, including Cr(110) [13–17,29,33–35,38–42], W(100) [43,44], Re(0001) [45], Rh [36], Pt(111) [46,47], Pd(111) [48], Pt [49], Cu(110) [50], Cu(100) [51], Cu(111) [52], Ag(111) [53], Au(111) [54], Fe(100) [55], Fe(110) [56], polycrystalline Fe [57], polycrystalline Co [57], polycrystalline Ni₈₀Fe₂₀ [57], NiAl₂O₄ [58], Fe₂O₃ [20,59–61], CrO₂ [62,63], and on sapphire or Al₂O₃(0001) [12,20–24,60,64–66].

We report here on chromia epitaxy on Cu(111), on Co(0001), and on graphitic carbon thin films, and compare our findings to films grown on Al₂O₃(0001) (sapphire), and to the broader body of literature just mentioned. Our study goes beyond earlier published studies as the result of the comprehensive suite of experimental methods used, combining sub-nanometer resolution imaging with electron diffraction and spectroscopy methods. X-ray photoelectron spectroscopy (XPS), and low energy electron diffraction (LEED) results indicate that for Cu and Co substrates, as well as for sapphire, continuous highly ordered films are formed with average thicknesses <20 Å. On cobalt, twinning of the chromia is likely to be common as the symmetry of the cobalt surface is C_{6v} (six fold), if the underlayer is not considered, and thus is not C_{3v} (three fold) like chromia. Such twinning is likely to occur, as well, on many other metal substrates, although apparently less likely on Cu(111). In the case of Cr₂O₃/Co(0001), a thin interfacial Co oxide is also formed, which is stable upon annealing or exposure to ambient. This is not enough to demonstrate the efficacy in a spintronics device application, although there remain promising indicators. The performance of envisioned magnetic tunnel junction structures [4,6,7] and spin field effect transistors [8–11], that seek to exploit the magneto-electric character of a material like chromia [2], would likely be enhanced by a stable chromia interface, both top and bottom, that is a continuous dielectric and magneto-

electric thin film. In this regard, there have also been studies of both copper [45,67] and cobalt growth [54,57,68] on chromia, pertinent to the work we report here. For chromia grown on graphite, however, formation of a completely oxidized but disordered chromia layer is achieved at 500 K. Subsequent annealing in UHV to >800 K results in the catalytic etching and removal of the graphitic layer.

2. Experiment

All experiments were performed in ultra-high vacuum (UHV, ~10⁻¹⁰ Torr) using 3 separate UHV systems, to make use of a broad range of surface analytic tools. System 1 was equipped with an Omicron Low-temperature scanning tunneling microscope (LT-STM). System 2 combined X-ray photoemission with an Omicron reverse view low energy electron diffraction (LEED) system [69]. This system has an introduction chamber (base pressure 1 × 10⁻⁷ Torr) with capabilities for magnetron sputter deposition from a graphite or Cr source, followed by sample transfer to the UHV chamber for LEED and XPS characterization without exposure to ambient. System 3 combined Auger electron spectroscopy (AES) and LEED as described previously [70]. Samples were either grown and studied in-situ, or transferred between systems through air where indicated, and surface contamination removed.

Chromia was deposited on four different substrates, crystalline Cu(111), thick epitaxial Co films sputter deposited on alumina substrates, graphitic carbon and Al₂O₃(0001) (sapphire). Different growth protocols for chromia were followed. It needs to be understood that each deposition method has advantages and disadvantages. The growth of chromia through chromium evaporation and subsequent oxidation is compatible with full ultrahigh vacuum and ideal for growing ultra-thin chromia films, but only so long as the adlayer of chromium does not alloy or dissolve into the substrate. Pulsed laser deposition is suitable for the growth of chromia thin films, especially growing a doped chromia, Cr₂B_xO_{3-x}, thin film [66]. The pulsed laser deposition of chromia is generally limited to growing thin films over small areas, however, and unlikely to be industrially scalable in the near future. Magnetron sputtering, as used on three of the four substrates studied, is industrially scalable, but rarely ultrahigh vacuum compatible.

- (i) Cu(111): Due to the dielectric nature of chromia, the scanning tunneling measurements required fine control of film thickness and very thin films, not possible by magnetron sputtering. As a consequence, the growth of chromia through chromium evaporation and subsequent oxidation compatible with ultrahigh vacuum was adopted for the STM studies on Cu(111). The Cu(111) single crystal of purity >99.999% was prepared by repeated cycles of Ar ion sputtering and annealing at 850 K in the preparation chamber. Metallic chromium was deposited on clean Cu(111) surfaces from an e-beam heated crucible. Chromia thin films were formed by post-annealing of the MBE-deposited Cr/Cu(111) sample at 923 K in a 5 × 10⁻⁷ mbar oxygen partial pressure for 1 min.
- (ii) Co(0001): The Co(0001) substrates were prepared ex-situ by magnetron sputter deposition onto Al₂O₃(0001) in presence of 15 mTorr Ar pressure, with an estimated Co thickness greater than ~1000 Å. In the chromia growth chamber, the Co(0001) film was annealed to 1000 K in presence of H₂ (1 × 10⁻⁶ Torr) in order to remove any dissolved oxygen from the bulk of Co, and further characterized by LEED and Auger electron spectroscopy (AES) prior to Cr deposition. Cr deposition was carried out using a commercial electron beam evaporator for MBE. Cr rod was used as the source and the chamber base pressure during deposition was less than

1×10^{-8} Torr. Cr_2O_3 was deposited by initiating Cr deposition in presence of 1×10^{-6} Torr O_2 at room temperature and subsequent annealing at 1000 K in 1×10^{-7} Torr O_2 .

- (iii) Graphitic carbon: Graphitic carbon was grown by magnetron sputter deposition from a graphite target in the introduction chamber (base pressure 1×10^{-7} Torr) onto a ~ 1000 Å thick Co(0001) sample, using a 4 mTorr Ar plasma with a sample temperature of 1000 K. This resulted in a ~ 19 Å graphitic carbon overlayer on the Co(0001)/ Al_2O_3 sample, as determined by XPS, and Raman. To grow a chromia layer on the graphitic carbon layer, the Cr sputter deposition at 500 K was followed by exposure to O_2 at or above room temperature, and annealing in UHV to order the film.
- (iv) Chromia on $\text{Al}_2\text{O}_3(0001)$ (sapphire) was grown by two methods. One approach was magnetron sputter deposition in the introduction chamber (base pressure 1×10^{-7} Torr) with a (Ar + O_2) gas mixture, with a relative Ar: O_2 pressure ratio of 1:9 at 500 K. Commercially available $\text{Al}_2\text{O}_3(0001)$ was used as the substrate. Subsequent annealing at 850 K in UHV produced an ordered Cr_2O_3 film on alumina. The other approach was pulsed laser deposition of Cr_2O_3 from a chromia target. We used a KrF excimer laser with pulse energies of 200 mJ and pulse width of 20 ns at a repetition rate of 10 Hz to create a plume from a chromia target allowing to deposit (0001) textured chromia thin films on cleaned sapphire (0001) substrates. The substrates were kept at 700 °C (973 K) during deposition and were located ~ 8.5 cm from the target. As mentioned above, this pulsed laser deposition approach was particularly successful for the fabrication of a boron doped chromia, $\text{Cr}_2\text{B}_x\text{O}_{3-x}$, important to raising the Néel temperature. Here pulsed laser deposition of Cr_2O_3 from a chromia target in the presence of $\text{B}_{10}\text{H}_{14}$ background atmosphere leads to substitution of O^{2-} ions by boron [66].

What emerges throughout this multitechnique comparison is that regardless of deposition method, chromia growth is robust, and always heavily textured towards growth along the $\langle 0001 \rangle$ direction.

Scanning tunneling microscopy (STM) studies of chromia films grown on Cu(111) were carried out using a low-temperature Omicron Nanotechnology STM. All STM studies shown in this paper have been performed at 77 K sample temperature.

The X-ray photoemission studies of chromia on Cu(111) were completed using both an aluminum anode with a $K\alpha$ of 1.486 keV and a magnesium anode with a $K\alpha$ of 1.254 keV photon energies, and with the photoelectron energy distribution curves measured with a hemispherical electron energy analyzer from Thermo VG Scientific, model VG 100, using a pass energy of 100 eV in 0.1 eV steps. The Cr 2p and O 1s core level binding energies are referenced to the Fermi level or chemical potential, calibrated using a Au foil and the Cu(111) substrate. The temperature was monitored using a type K thermocouple and cross-checked using an infrared pyrometer.

XPS spectra of chromia on Co(0001) or graphene/graphite were acquired with a 100 mm mean radius hemispherical analyzer operated in constant pass energy mode (22 eV), and an unmonochromatized Mg $K\alpha$ x-ray source (photon energy 1253.6 keV) operated at 300 W. AES spectra of chromia on Co(0001) were acquired by a cylindrical mirror analyzer with co-axial electron gun, operated at 3 keV. LEED data for these films were obtained using commercially available reverse-view LEED instruments. The average thicknesses and stoichiometries of chromia films on Co or graphene/graphite were derived from XPS or AES data using standard methods.

3. Chromia growth on Cu(111)

Fig. 1a shows an STM image of a nominally 2 monolayer (ML), MBE-deposited Cr film on Cu(111). As shown in Fig. 1, the hetero-epitaxy of the as-deposited chromium metal film follows the Volmer–Weber, or island growth mode on Cu(111), where small clusters 2–5 nm in diameter decorate step edges and terraces.

Upon annealing the deposited Cr on Cu(111) in a 10^{-7} Torr O_2 partial pressure at 923 K, the adlayer topography changes considerably. The STM topography images of the oxygen-annealed film in Fig. 1b reveal that the small chromium islands coalesce to form large, flat terraces that cross several Cu(111) terraces. The apparent height of the oxide film is about 2 nm. This considerable increase in film thickness is the result of island ripening and partial de-wetting of the Cu(111) surface, in combination with oxygen uptake by the Cr. Visible within the large flat islands are small steps of apparent step height of 1 Å. This step height deviates considerably from the distance between two equivalent (0001) surface terminations of α - $\text{Cr}_2\text{O}_3(0001)$, which are separated by a monoatomic step with a height of 2.3 Å. However, it should be noted that precise height measurements on chromia films with STM is problematic due to the insulating nature of $\text{Cr}_2\text{O}_3(0001)$, which makes the films effectively part of the tunnel barrier. This method is only suitable for the growth of thinner Cr_2O_3 films, as applicability is limited by the ability of oxygen to penetrate the Cr during annealing. It is after all, the formation of chromia that provides the corrosion barrier that makes stainless steel or inox steel, “stainless” [71–76]. This oxide film, or passivating boundary layer, is typically very thin (of order 2–3 nm). Thicker films grown by evaporation of chromium and subsequent oxidation would require repetitive cycles of chromium thin film evaporation and oxidation.

In order to check the chemical composition and structure of the chromium oxide film, XPS and LEED measurements were performed on the sample. Fig. 2 shows both the Cr 2p and O 1s core level photoemission data taken at room temperature, with a 20° degree emission angle with respect to the surface normal, after the sample was annealed in UHV at 600 K for 20 min to remove contaminants. Since the chromia film is quite thin, with monolayer coverage at about 1 unit cell height, the small signal-to-noise ratio for Cr 2p spectra is expected. Using the peak maximum or as appropriate, the maximum of the various peak fit to the spectra, the binding energies were established, and surface sensitivity ascertained the relative intensity of the features as a function of the photoemission emission angle. On this basis, the binding energy of the Cr $2p_{3/2}$ core level is 576.2 ± 0.1 eV, a clear shift from the metallic chromium peak found at 574.4 eV, and in agreement with previously published values for thicker chromia films on Cu(111) [52]. The Cr $2p_{3/2}$ –Cr $2p_{1/2}$ binding energy separation is 9.5 eV, which is also very close to the reported binding energy separation for Cr_2O_3 and other single phase chromium species [52,64]. The binding energy of the O 1s core level (Fig. 2) for the annealed sample is 530.4 ± 0.2 eV, in agreement with that reported for a very thin film on Cu(111) (530.4 eV) [52]. This suggests that the O 1s spectrum (Fig. 2b) contains a component with a peak at 532.8 ± 0.3 eV and a component that could well be representative of the surface rather than the interface of the Cr_2O_3 with copper, where the well screened final state is expected to place the oxygen core level closer to 530.2 eV. This higher binding energy component of the O 1s core level spectra is seen to increase in relative intensity with increasing take off angle, thus indicative of greater localization at the surface, as opposed to the bulk of the chromia film. Chromia does have a surface state [1], and surface to bulk core level shifts, for the metal core, are known even for even the most dielectric oxides [77,78], as are final state screening effects [79]. These chromia core level binding energies are very much in line with expectations

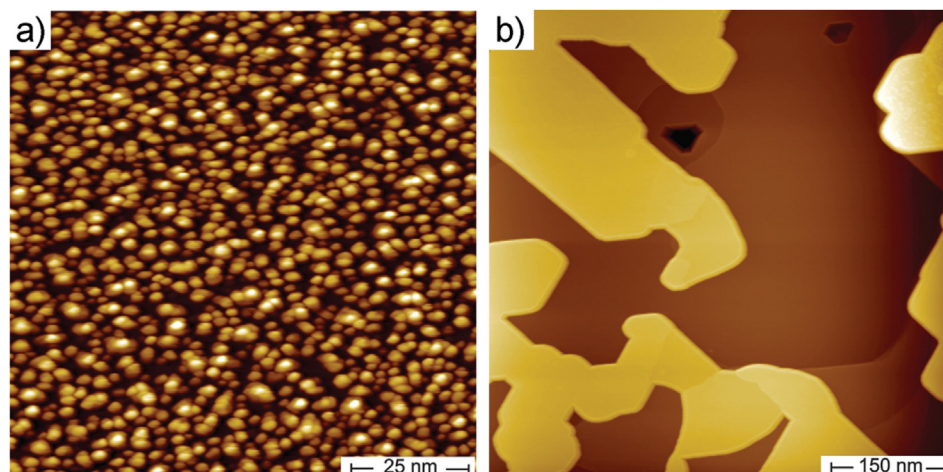


Fig. 1. (a) The STM topographic image of 2 monolayers (ML) Cr deposited on Cu(111) at room temperature. (b) STM topographic image of the chromium oxide film formed by annealing 2 ML Cr/Cu(111) sample in a 5×10^{-7} mbar oxygen atmosphere at 920 K for 1 min (see text).

based on previously reported results (Table 1). We thus conclude that the flat film observed is indeed a chromia adlayer.

The low energy electron diffraction (LEED) studies establish that this chromia film exhibits a dominant (0001) texture with very little mosaic spread. The LEED pattern for the chromia film on Cu(111) (Fig. 3a) exhibits an overall hexagonal diffraction pattern with C_{3v} symmetry. This further supports the contention that the film is Cr_2O_3 in a single phase and single domain. This LEED demonstrates that the chromia adlayer has adopted (0001) texture growth, but with surprisingly very little mosaic spread, i.e. $\alpha\text{-Cr}_2\text{O}_3(0001)$. While Cu(111) and Co(111) are closely lattice matched, the lattice match with chromia is imperfect, as noted elsewhere in studies of copper deposition on chromia [45,67]. Consistent with these earlier studies, we find that Cu will also adopt (111) texture growth on $\alpha\text{-Cr}_2\text{O}_3(0001)$, but with a lattice mismatch, as is clearly evident of the LEED of Fig. 3b.

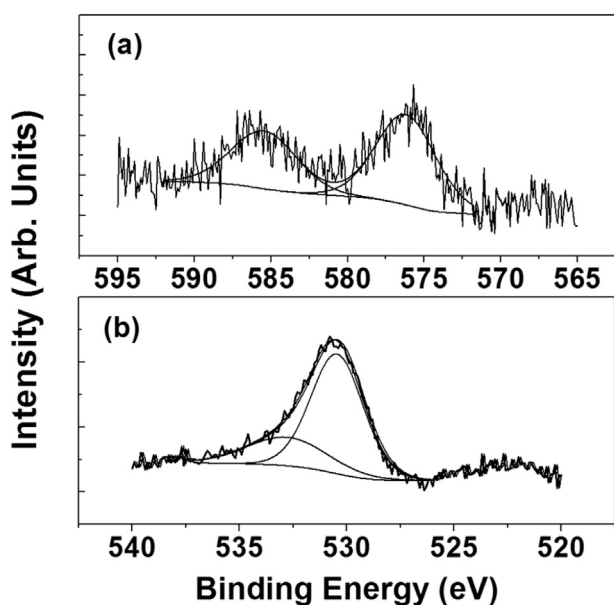


Fig. 2. The XPS spectra (a) Cr 2p and (b) O 1s at 20° emission angle, with respect to the surface normal, for a chromia adlayer on Cu(111). Binding energies denoted as E_F -E. The smooth lines are peak fitting results.

4. Chromia growth on Co(0001)

Fig. 4a displays Auger electron spectroscopy (AES) acquired after the first (solid line) and second (dashed line) Cr deposition/oxidation cycles on Co(0001). The Cr(LMM) and O(KVV) spectra (Fig. 4a,b) are consistent with Cr_2O_3 [55,58,80] and indicate an average chromia thickness of 9 Å after the first deposition/oxidation cycle, and 11 Å average thickness after the second deposition/oxidation cycle. This apparent change in deposition rate between cycles may be due in part to small variations in sample position and beam flux, but may also reflect a change in Cr sticking coefficient with chromia surface coverage. The corresponding low energy LEED image (Fig. 5a) and corresponding line scan (Fig. 5b) for the 9 Å chromia film consists of a faint outer six-fold array of diffraction spots, and a brighter inner array of six-fold LEED diffraction spots, both arrays having the same angular orientation. After the 2nd deposition, however, the LEED image (Fig. 5c) and corresponding line scan (Fig. 5d) across the LEED image, taken for 11 Å of chromia on Co(0001), indicate only the inner ring of LEED diffraction spots. The outer ring of LEED diffraction spots has disappeared. This identifies the outer LEED diffraction spots in Fig. 5a array as related to a six-fold Co(0001) substrate and the inner LEED diffraction spots as corresponding to Cr_2O_3 . The absence of substrate-related spots after the second deposition (Fig. 5c,d) indicates that two deposition/oxidation cycles result in a continuous, epitaxial chromia film on Co(0001), much like that observed for chromia on Cu(111), as discussed above. The LEED patterns for chromia on Co(0001) (Fig. 5a,c) do not, however, exhibit C_{3v} symmetry, indicating that the film is not single-domain. From X-ray ϕ scans it is known that the chromia (0001) surfaces tend to have twin domains, and such twinning is likely, and a possible explanation for the 6 fold, rather than 3 fold, symmetry. These LEED images for chromia on Co(0001) (Fig. 5a,c) are similar to those previously reported for $\text{Cr}_2\text{O}_3(0001)$ films on Ag(111) [53]. Although there is a lattice mismatch, a comparison of chromia LEED diffraction spots, with those from the Co substrate (Fig. 5a), indicate that the lattice of the chromia overlayer and Co substrate are aligned.

The XPS Cr 2p and O 1s spectra of chromia (Cr_2O_3) grown on Co(0001) are shown in Fig. 6a,b. The corresponding LEED image for the chromia/Co film, after a flash anneal in ultra high vacuum (UHV), is shown in Fig. 7a, while that of a clean Co(0001) substrate acquired in the same chamber under the same experimental conditions is shown in Fig. 7b. Corresponding LEED images for the

Table 1

Comparison of Cr(2p)_{3/2} and Cr(2p)_{1/2} binding energy values for Cr₂O₃ films grown on Cu(111), Co(0001), Al₂O₃(0001) and graphitic carbon versus literature values. Binding energy refers to the peak maximum and are in units of [eV].

Substrate	Cr (2p _{1/2})	Cr (2p _{3/2})	O (1s)	Cr (2p _{3/2}) – O (1s) binding energy difference
Cu(111)	585.7 ± 0.3 ^{this work}	576.1 ± 0.2 ^{this work}	530.4 ± 0.2 ^{this work}	45.7
		–	532.8 ± 0.3 ^{this work}	45.8
		576.2 [52]	530.4 [52]	
Cu(110)	–	577.0 [50]	530.6 ± 0.2 [50]	46.4
Cu(100)	–	577.0 [51]	–	–
Ag(111)	584 [53]	–	531 [53]	–
Pd(111)	586.6 ± 0.1 [48]	576.8 ± 0.1 [48]	–	–
Pt(111)	–	577.0 [46]	–	–
		577.0 [47]	–	–
Co(0001)	585.4 ± 0.2 ^{this work}	575.7 ± 0.2 ^{this work}	529.6 ± 0.2 ^{this work}	46.1
Cr(110)	–	576.6 [40]	531.5 [40]	45.1
		577.0 [41]	–	–
W(100)	585.8 [44]	576.3 [44]	530.5 [44]	45.8
Rh	586.8 ± 0.2 [36]	576.8 [36]	–	–
Re(0001)	586.5 [45]	576.7 [45]	530.2 [45]	46.5
Graphitic carbon	585.3 ± 0.2 ^{this work}	575.6 ± 0.2 ^{this work}	528.8 ± 0.2 ^{this work}	46.8
NiAl ₂ O ₄	586.9 [58]	577.2 [58]	530.5 [58]	46.7
CrO ₂	586.5 ± 0.3 [62]	576.8 ± 0.2 [62,68]	531.1 ± 0.2 [62]	45.7
	585.2 ± 0.2 [63]	575.7 ± 0.2 [63]	–	–
Al ₂ O ₃ (0001)	585.9 ± 0.2 ^{this work}	576.2 ± 0.2 ^{this work}	530 ± 0.2 ^{this work}	46.2
Bulk Cr ₂ O ₃	585.9 ± 0.2 [63]	576.0 ± 0.2 [63,71]	531.1 ^{this work}	45.7
		575.6 [71]	533 ^{this work}	45.4
		575.7 [72]	529.9 [71]	–
		576.3 [73,74]	530.3 [72,76]	–
		576.5 [75]	531.5 [95]	–

chromia film on Al₂O₃(0001), and the alumina substrate prior to chromia deposition, are shown in Fig. 7c,d for comparison.

The Cr₂O₃(0001)/Co(0001) LEED diffraction image (Fig. 5c) is stable after exposure to air, transfer and annealing (Fig. 7a), so even for a more reactive substrate like Co(0001), sample transfer will not significantly disrupt the long range order of the chromia film.

As shown in Fig. 6a,b, the XPS Cr 2p_{3/2} and O 1s spectra, for the ~11 Å thick chromia films on Co(0001), exhibit peak maxima at binding energies of 575.7 eV and 529.6 eV, rather smaller than those observed for chromia on most other substrates (Table 1). For chromia on Co(0001) experiments, the XPS peaks were referenced to a metallic Co 2p_{3/2} peak binding energy of 778.1 eV [81,82] obtained from the ~1000 Å thick Co substrate. These data exhibit core level binding energies greater than those observed for chromia on sapphire (Fig. 6c,d). For chromia on Al₂O₃, the core level photoemission peaks were referenced with respect to the Al 2p_{3/2} peak at 74.7 eV [81,83], but there is considerable uncertainty as to the correct Al 2p reference binding energy because this is a dielectric substrate and is reflected by the range of binding energies reported from 73.5 eV [84], to 73.7 eV [85] to 74.1 eV [86] to 74.9 eV [82].

Thus, there is no certainty that the greater binding energy is due to the dielectric substrate or the greater chromia film thickness. The XPS indicates the average thickness of the Cr₂O₃ film on alumina is 25 Å. The thicker chromia film on alumina exhibits higher binding energies compared to the 11 Å thick Cr₂O₃ film on Co(0001).

The Co 2p XPS spectra for the Cr₂O₃/Co(0001) film (Fig. 8) also show a high binding energy shoulder, indicating the presence of an interfacial Co oxide with an average thickness of 3.5 Å. This oxide layer showed no change upon subsequent sample exposures to ambient air and annealing in UHV, providing additional evidence for the continuity of the chromia overlayer. This is consistent with our observation that the Cr₂O₃(0001)/Co(0001) LEED diffraction images, are stable after exposure to air, during transfer, and subsequent annealing, so even for a more reactive substrate like Co(0001), sample transfer will not significantly disrupt the long range order of the chromia film. This interfacial oxidation at the cobalt to chromia interface has also been seen for cobalt deposition on chromia [68], and could contribute to the formation of chromia twinning and loss of C_{3v} symmetry, compared to chromia growth on Cu(111).

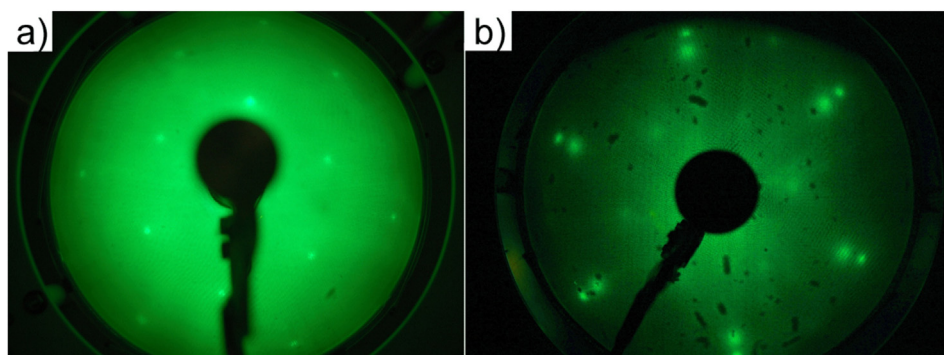


Fig. 3. (a) The LEED for a chromia adlayer on Cu(111) (see text). The LEED kinetic energy is 260 eV. (b) The LEED showing the strong ordering of Cu(111) on a single crystal of α -Cr₂O₃(0001) at 684 K. The LEED pattern was taken at incident electron energy of 70 eV.

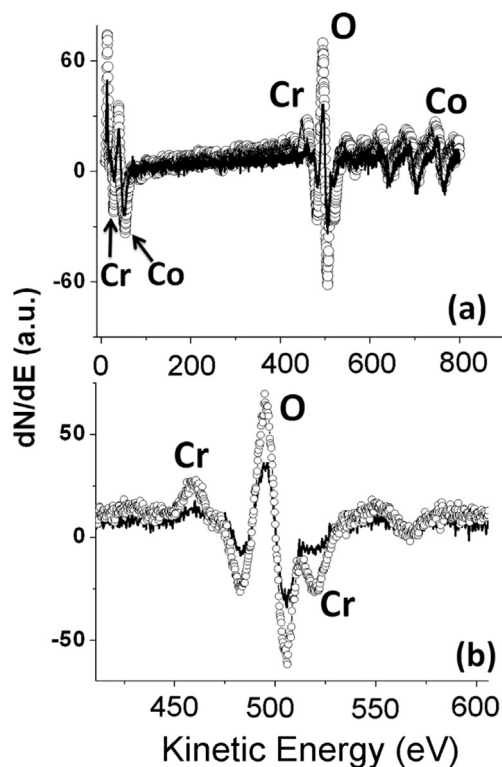


Fig. 4. (a) Auger electron spectroscopy acquired after 1st Cr MBE/oxidation cycle (solid black trace) and after 2nd Cr MBE/oxidation cycle (open circles), (b) the expanded view of the Cr(LMM)/O(KVV) region. (LMM is an L shell core hole, M shell transition and M shell Auger electron while KVV is a K shell core hole, transition from the valence band and valence band Auger electron).

5. Chromia growth on $\text{Al}_2\text{O}_3(0001)$

It should be noted that sapphire is the frequent substrate of choice [12,20–24,60,64,65] for chromia growth because of the close lattice match to $\alpha\text{-Al}_2\text{O}_3(0001)$ substrate. This is borne out in our LEED studies as well. The LEED image for the chromia/alumina film (Fig. 7c) exhibits C_{3v} symmetry, indicating that the film grown on alumina occurs in a single domain film, or at least twinning of the chromia is vastly suppressed and that the chromia lattice is aligned with that of the $\text{Al}_2\text{O}_3(0001)$ substrate, as noted by many previous investigators [12,20–24,60,64,65]. This is in contrast to LEED images for $\text{Cr}_2\text{O}_3(0001)/\text{Co}(0001)$ (Fig. 5a,c and 7a), that exhibit six-fold symmetry. This indicates that the chromia film grown on alumina, as with the film grown on Cu(111) is single domain, but that the films grown on Co almost certainly not single domain.

It is clear that a lattice match for chromia growth, with regard to the substrate, is not essential. In particular, the lattice match for chromia growth on $\text{Al}_2\text{O}_3(0001)$ is not perfect and thicker chromia films do not share the same lattice constant with the alumina substrate [66], as seen in Fig. 9. These pulse laser deposition films are seen to be very flat, with a roughness of 0.22 nm or less, in spite of the lattice mismatch between the substrate and chromia overlayer. We note that textured growth of chromia with an (1–102) was observed on an Al_2O_3 substrate also of (1–102) orientation [87]. Again, perfect lattice match was not observed, and some growth included grains with other orientations [87]. What this means is that while texture growth of chromia along (0001) is common, and perhaps often dominant, the substrate can influence the texture for growth along other orientations.

6. Chromia growth on graphitic carbon by physical vapor deposition

The tendency for chromia growth to favor (0001) texture growth is evident in the growth of chromia on graphitic carbon. The

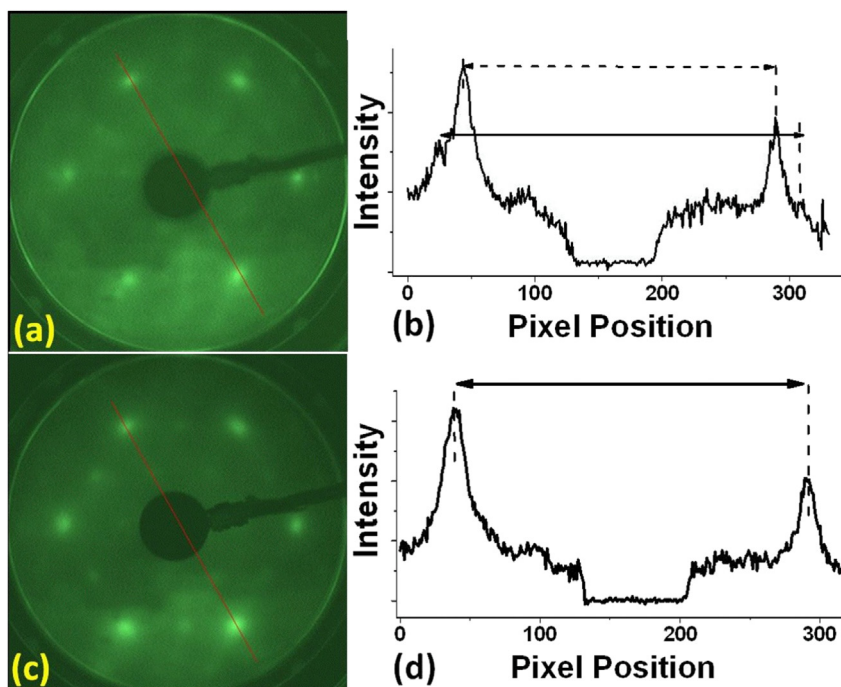


Fig. 5. The LEED image (a) and line scan (b) after the first chromium deposition/oxidation cycle (roughly 9 Å) on Co(0001). Note the evidence of overlayer mismatch in the line scan. This can be compared with the LEED image (c) and line scan (d) after second chromium deposition/oxidation cycle (roughly 11 Å) on Co(0001). Note that the outer ring of LEED diffraction spots identified in the line scan of b is related to a six-fold Co(0001) substrate, and is not evident with thicker chromia overlayers (d). The LEED electron beam energy is 90 eV. Dashed and solid lines in (b,d) are guides to the eye.

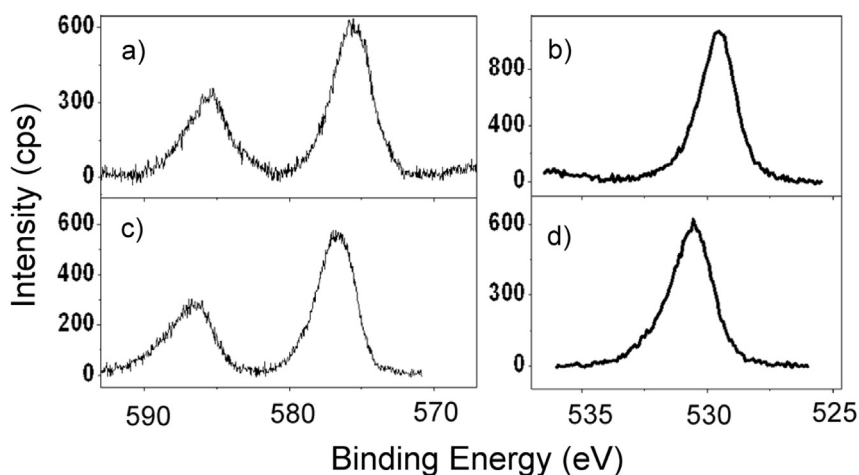


Fig. 6. The XPS core level spectra for Cr 2p (a) and O 1s (b) core levels after Cr₂O₃ deposition on Co(0001) (see text), and for Cr 2p (c) and O 1s (c) core levels after Cr₂O₃ deposition on Al₂O₃.

XPS data for the graphitic film prior to chromium deposition (Fig. 10a), after deposition and partial oxidation of chromium (Fig. 10b), and after further oxidation and annealing to 800 K in UHV (Fig. 10c) show that coexistence of a suboxide and chromia are possible. The corresponding LEED image data are displayed in Fig. 11a–c, respectively.

Prior to Cr deposition, the XPS data (Fig. 10a) indicate a C 1s feature with a binding energy near 284.5 eV, indicative of negligible carbon oxidation, and an average C overlayer thickness of 19 Å. The three cycles of Cr deposition at 500 K followed by room temperature oxidation (2 mTorr for 10 min each cycle) resulted in a partially oxidized, hexagonally ordered chromia film, ~7 Å average

thickness, as indicated by the core level XPS spectra in Fig. 10b, and corresponding LEED image (Fig. 10b). The Cr 2p core level XPS feature (Fig. 10b) exhibits a maximum at 575.6 eV, but with a pronounced shoulder at lower binding energy indicating the presence of chromium in a metallic or suboxide state. Consistent with our expectations as to how the chromium oxidation proceeds, emission angle dependent XPS Cr 2p spectra (Fig. 12) indicate that metallic chromium is at the interface between the chromia and the graphite layer, not the surface. Subsequent oxidation at 500 K resulted in elimination of the low binding energy shoulder, indicating complete oxidation to Cr₂O₃, but with no observable LEED pattern. Annealing the chromia film to 800 K in UHV, however,

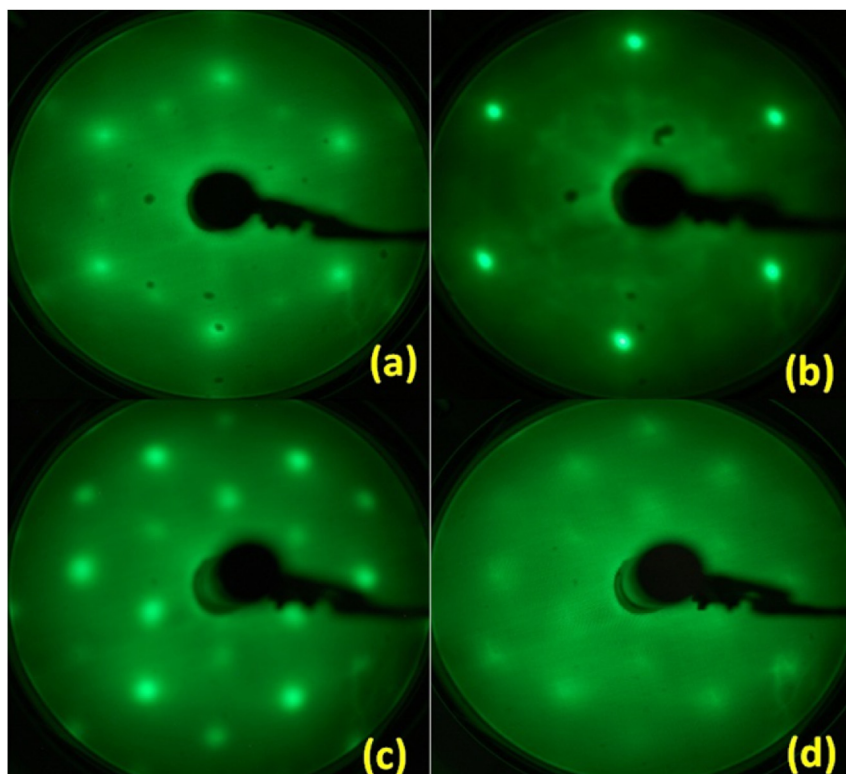


Fig. 7. The various LEED patterns for chromia overlayers on cobalt and sapphire: (a) thicker (>11 Å) Cr₂O₃ on Co; (b) the clean Co substrate; (c) Cr₂O₃ on Al₂O₃ (d) the clean Al₂O₃ substrate; All LEED patterns acquired at 90 eV beam kinetic energy.

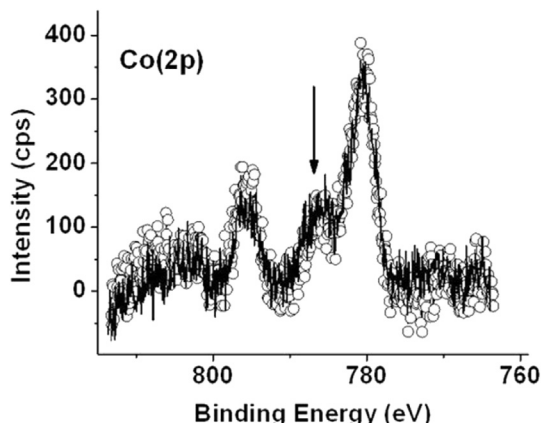


Fig. 8. XPS Co 2p spectra of a $\text{Cr}_2\text{O}_3(0001)/\text{Co}(0001)$ film after sample transfer/UHV anneal (solid trace) and after a second air exposure/UHV annealing cycle (open circle). The feature corresponding to the presence of cobalt oxide is marked by an arrow.

resulted in the degradation and removal of the graphitic C layer, as evidenced by the lack of resulting C 1s intensity (Fig. 10c) and a six fold LEED pattern indicative of an ordered chromia adlayer (Fig. 11c). Since annealing the Cr metal/graphite interface in UHV did not yield carbon dissolution, the data in Figs. 10 and 11 indicate that catalytic etching of the graphitic layer, by chromia, occurred at temperatures >800 K. This suggests practical thermal limits to the annealing of chromia layers on graphitic carbon, even under UHV conditions.

The LEED image (Fig. 11a) indicates that presence of graphitic domains or layers azimuthally rotated with respect to each other, as was observed with graphene/SiC [88]. This disorder in the graphitic carbon layer does not translate to a hugely disordered chromia layer; rather strong (0001) basal face texture growth of the chromia layer is again evident as seen in Fig. 11b,c.

7. Discussion

Regardless of deposition method, the growth of chromia, Cr_2O_3 , thin film is robust. The data presented here demonstrate that while there is some influence of substrate reactivity on chromia growth and stability, chromia thin film growth on a variety of substrates favors the (0001) basal face texture growth direction. In all cases examined here, the orientation of the Cr_2O_3 lattice is aligned with that of the substrate. Growth of Cr_2O_3 on Cu(111), as on Pt [46,47] or on Ag(111) [53], can yield quasi-epitaxial growth (single phase chromia domain growth, but perhaps without a perfect lattice

match), with an atomically abrupt interface. Indeed, it is interesting that oxidation of Cr on Cu(111) at ~ 920 K in UHV enhances film wetting of the substrate, consistent with previously reported results [51]. In contrast, chromia de-wetting from Pt(111) is observed at >700 K [47]. Cr_2O_3 films grown on Co(0001) are also stable at temperatures larger than 1000 K, but this may be due to the formation of an interfacial Co oxide. The formation of an ultrathin Co oxide interface may be of relevance for spintronics applications. Studies of the magnetic properties of ordered Co layers on $\text{Cr}_2\text{O}_3(0001)$ have been reported [60,64,75], but interface effects on the perpendicular magnetic anisotropy and the exchange bias will depend greatly on the interface and interface composition. An abrupt Co/chromia interface (no interfacial Co oxide) cannot be assumed: the results reported here suggest that ultrathin interfacial Co oxides may be formed under appropriate conditions, and their existence should be considered in the investigation of magnetic properties of such heterostructures.

Cr_2O_3 growth on graphene or graphite is of interest due to the possibility of using a voltage-switchable magnetoelectric material for proximity-induced polarization of graphene [8–11,89,90] and use of the chromia as a dielectric gate with high interface polarization [1,2]. The data reported here, however, indicate that such a task may be difficult owing to the potential for chromia catalyzed oxidation of the carbon substrate. Chromia catalysis of hydrocarbon oxidation is well-documented [91], and the data here suggest that any chromia growth on graphite or graphene should occur at <800 K. Since annealing of the graphitic layer to >800 K in the presence of either UHV or metallic Cr yielded no observable change in the graphite layer, the disappearance of the C 1s signal upon annealing in the presence of chromia (Fig. 9c) indicates that this effect is likely not due to C dissolution into the Co substrate, but rather to the catalytic oxidation and possible desorption of the carbon layer. Catalyzed destruction of graphitic carbon by chromia remains a concern, and suggests that chromia growth on graphene, or direct graphene growth on chromia is problematic.

The Cr 2p core level XPS binding energies are obviously a major indicator of the presence of Cr^{+3} ions, and the formation of Cr_2O_3 , as opposed to Cr_3O_4 or other phases. The reported chromium $2p_{3/2}$ binding energies for the Cr_2O_3 oxide fall into two groups: those that range from 575.7 eV to 576.3 eV (this work and references [44,52,63,71–74]), and those that range from 576.8 eV to 577.2 eV (references [46–48,50,51,62,68]), as seen in Table 1. It should be noted that the publications reporting the larger binding energies also report a lower binding energy component of 575.8 eV [51], 576 eV [41,50], 576.5 eV [46,47]. Frequently, the two components have been ascribed to Cr^{+2} and Cr^{+3} [41,45,46,50,51], but a surface to bulk core level shift, in the photoemission final state, is (in our

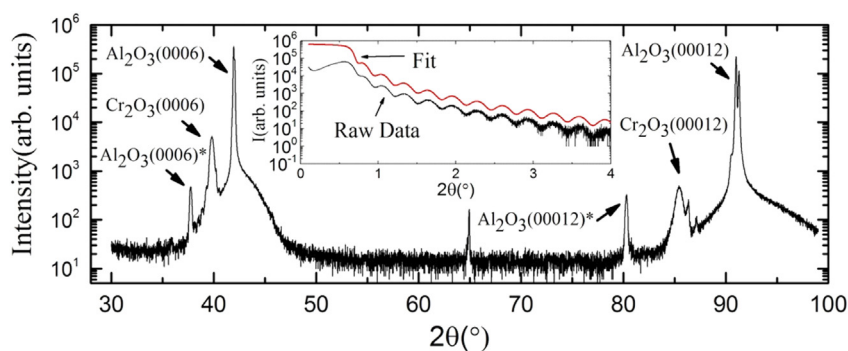


Fig. 9. Wide and small angle x-ray diffraction of pure chromia thin films grown by pulsed laser deposition on alumina. Narrow (0006) and (00012) K_z peaks indicate (0001) textured chromia. (*) indicates K_β peaks. The inset shows small angle x-ray diffraction raw data and best fit (shifted for clarity relative to raw data) determining a film thickness of 26.3 nm and roughness of 0.22 nm. Adapted from [66].

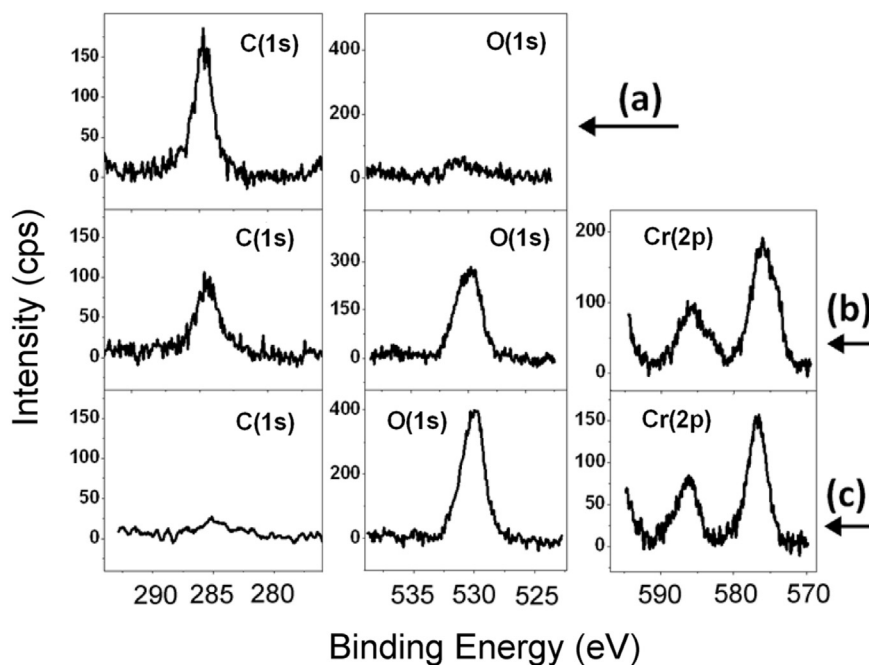


Fig. 10. XPS core spectra of C(1s), O(1s) and Cr(2p) for deposition of graphitic carbon on Co/Al₂O₃ substrate (row: a), after deposition of Cr₂O₃ on graphitic carbon/Co/Al₂O₃ substrate (row: b), and annealed at 800 K, after deposition of Cr₂O₃ on the graphitic carbon/Co/Al₂O₃ substrate (row: c).

opinion) equally or even more plausible given that chromia has a surface state [1]. Our observation that both chromium bulk crystals and chromia thin films exhibit a “surface” and “bulk” component, in the O 1s core level spectra is consistent with a surface to bulk core level shift or differences in binding energy due to difference in the photoemission final state.

Both chromium 2p_{3/2} binding energy components for the Cr₂O₃ oxide occur at much higher binding energies than expected for the chromium metal e.g. 573.6 eV [71], 574.0 eV [76,92], 574.1 eV [52,73,74,93–95], 574.2 eV [41], 574.4 eV [40]. This, together with observation [52] that thicker chromia films exhibit higher Cr 2p_{3/2} binding energies, suggests that final state screening may play a significant role, rather than initial state chemical oxidation. Such a final state effect could result from a surface to core level shift, common for oxides, although difficult to distinguish between a different initial chemical state at the surface, or different screening as a result of the final state screening that might occur from the metallic substrate screening the Cr⁺³ photoemission final state. For the Cr 2p_{3/2} binding energies reported for chromia thin films on metals, that group at smaller binding energies in fact are consistent

with the chromia formed at the surface of many stainless steels [71,73–75], as summarized in Table 1, and this chromia is typically quite thin, no more than a few nanometers at most, as mentioned above. For this reason, the approach of assigning the multiple core level binding energies of the Cr 2p_{3/2}, to different chromium oxidation states, at this junction, may have been too simplistic. Final state screening effect upon the Cr 2p_{3/2} core level binding energies should be considered, especially considering that the nominal band gap of the surface electronic structure is smaller than the bulk band gap of chromia [1]. This surmise that final state surface and bulk contributions, with different binding energies might contribute to the Cr 2p_{3/2} core level photoemission spectra under some conditions, is supported by angle-resolved high resolution core level photoemission studies of bulk chromia single crystals where the surface is seen to have a different binding energy than the bulk. The fact that sometimes the oxygen 1s core level binding energies is seen to have multiple components is also consistent with this assignment, as noted above, for the case of chromia thin films on copper, and bulk chromia single crystals as noted in the table below.

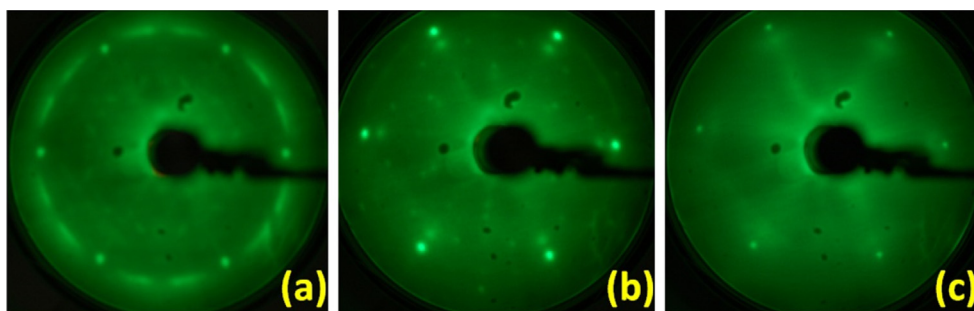


Fig. 11. LEED after (a) deposition of 2 nm of graphitic carbon on a Co/Al₂O₃ substrate, (b) after deposition of 12 Å Cr₂O₃ on 2 nm of graphitic carbon on a Co/Al₂O₃ substrate, and (c) after a subsequent anneal at 800 K after deposition of Cr₂O₃ on 2 nm of graphitic carbon on a Co/Al₂O₃ substrate. All the LEED images were taken with an electron kinetic energy of 90 eV.

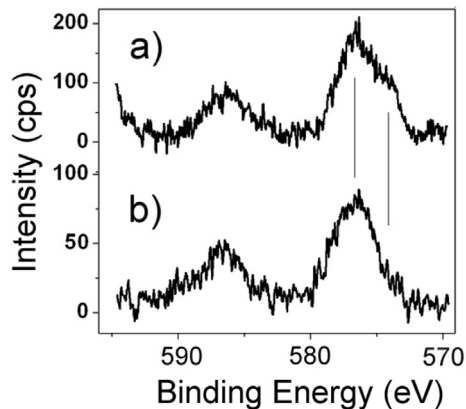


Fig. 12. The Cr 2p XPS spectra acquired with emission parallel to the sample normal (a) and at 60° relative to the sample normal (b), for a 12 Å film deposited on graphite at 500 K and then exposed to 2 mTorr O_2 at room temperature for 20 min. Lines are guides to the eye. Note that with the increasing emission angle (b), the Cr metal core level component decreases, indicating that the metallic chromium is below the oxide layer, in contact with the carbon substrate.

Without question, as noted in the introduction, exchange bias with the very thinnest chromia films (<2 nm) is not possible. Regular exchange bias requires the antiferromagnet to overcome some critical thickness, which is likely much larger than just one unit cell. Recent work, illustrates that texture growth along the chromia (1–102) direction will also lead to exchange bias [87], so even perfect texture growth is not required. Yet for most device implementation schemes, the chromia thin film should be pinhole free, so as to be able to use as a gate dielectric. Proof of a pin-hole free thin film, in the thin film limit, rests generally on transport measurements, with chromia as the dielectric in a tunnel junction structure as in [56,57,96–98], with compelling proof of chromia as a suitable dielectric in the thin film limit only for $CrO_2/Cr_2O_3/CrO_2$ structures [96–98].

8. Summary and conclusions

$Cr_2O_3(0001)$ texture growth is favored on many substrates, and generally robust regardless of lattice match. The STM, XPS and LEED data demonstrate that oxidation of a thin Cr overlayer at 1000 K yields an epitaxial, uniform single phase $Cr_2O_3(0001)$ layer 10 Å ~ 20 Å thick that wets the Cu(111) substrate, even if the deposition of chromium metal does not. Cr deposition/oxidation on Co(0001) also provides an Cr_2O_3 layer ~11 Å thick average thickness, even if not epitaxial, stable to >1000 K in ultra high vacuum (UHV), but accompanied by the formation of an interfacial Co oxide layer ~3.5 Å thick. In both cases, the orientation of the chromia lattice was aligned with that of the substrate, in spite of a lattice mismatch. A mixed chromia/Cr metal or incomplete chromia oxide phase, with hexagonal ordering, is formed by Cr deposition/oxidation on a graphitic substrate. The metallic or incompletely oxidized phases is at the oxide/graphite interface. Full oxidation of this layer, followed by annealing to >800 K in UHV resulted in etching of the graphitic carbon substrate.

The data demonstrate that ultrathin (<2 nm), continuous, epitaxial chromia films can be grown on Cu and on Co substrates, and that such films are stable to at least 1000 K in UHV. Of potential practical interest is the fact that such films, whether on Cu or on Co or indeed any other substrate, survive exposure to ambient air without significant change to chemical composition or long range order. Such stability does seem to occur, at least in some cases, suggesting the practicality of such heterostructures for spintronics and other applications. The advantages of Cu(111) and Co(111) are

that these are nonmagnetic and ferromagnetic metals, respectively, that closely lattice matched and can be grown on each other, with epitaxial growth, so the resulting Co(111) thin films exhibit low coercivity [99]. From the perspective of magneto-electric “gated” magnetic tunnel junction structure device [4,6,7], there is a disadvantage in using cobalt as the free magnetic layer in combination with chromia as cobalt thin films on copper have little perpendicular magnetic anisotropy [99,100]. Exploitation of voltage control of exchange bias by implementation of a soft free magnetic layer with perpendicular magnetic anisotropy, through the boundary magnetization of ultrathin chromia thin films, are challenges beyond the scope of this work and currently under investigation by a number of research groups. But key is that this work here demonstrates that epitaxial growth is by no means essential for thin film growth in combination with a magneto-electric oxide such as chromia. Without question, as noted in the introduction, exchange bias with the very thinnest chromia films (<2 nm) is not possible. Regular exchange bias requires the antiferromagnet to overcome some critical thickness, which is likely much larger than just one unit cell.

Acknowledgments

This work was supported by the Semiconductor Research Corporation under tasks 2123.001 and 2358.001, and by C-SPIN, part of STARnet, a Semiconductor Research Corporation program sponsored by MARCO and DARPA (SRC 2381.001) and by the Center for NanoFerroic Devices (CNFD) and the Semiconductor Research Corporation Nanoelectronics Research Initiative (NRI), tasks (SRC 2398.001). Further funding was provided through the Nebraska Center for Energy Sciences Research and through NSF Grant EPS-1004094 and the NSF funded Nebraska MRSEC DMR-0820521 and the Nebraska Center for Materials and Nanoscience (NCMN).

References

- [1] Xi He, Yi Wang, Ning Wu, A.N. Caruso, E. Vescovo, K.D. Belashchenko, P.A. Dowben, Ch Binek, *Nat. Mater.* 9 (2010) 579–585.
- [2] Ning Wu, Xi He, A. Wysocki, U. Lanke, T. Komesu, K.D. Belashchenko, Ch Binek, P.A. Dowben, *Phys. Rev. Lett.* 106 (2011) 087202.
- [3] W. Echtenkamp, Ch Binek, *Phys. Rev. Lett.* 111 (2013) 187204.
- [4] W. Kleemann, *J. Appl. Phys.* 114 (2013) 027013.
- [5] T. Ashida, Y. Sato, T. Nozaki, M. Sahashi, *J. Appl. Phys.* 113 (2013) 17D711.
- [6] Ch Binek, B. Doudin, *J. Phys. Condens. Matter* 17 (2005) L39–L44.
- [7] M. Bibes, A. Barthélémy, *Nat. Mater.* 7 (2008) 425–426.
- [8] H. Dery, P. Dalal, L. Cywiński, L.J. Sham, *Nature* 447 (2007) 573–576.
- [9] Y.G. Semenov, K.W. Kim, J.M. Zavada, *Appl. Phys. Lett.* 91 (2007) 153105.
- [10] I. Zaliznyak, A. Tselvik, D. Kharzeev, U.S. Patent Application US 2010/0109712 A1, May 6 2010.
- [11] Y.G. Semenov, J.M. Zavada, K.W. Kim, *J. Appl. Phys.* 107 (2010) 064507.
- [12] L. Fallarino, A. Berger, Ch Binek, *Appl. Phys. Lett.* 104 (2014) 022403.
- [13] M. Bender, O. Seiferth, A.F. Carley, A. Chambers, H.J. Freund, M.W. Roberts, *Surf. Sci.* 513 (2002) 221–232.
- [14] K. Al-Shamery, *Appl. Phys. A* 63 (1996) 509–521.
- [15] I. Beauport, K. Al-Shamery, H.J. Freund, *Surf. Sci.* 363 (1996) 252–261.
- [16] I. Beauport, K. Al-Shamery, H.J. Freund, *Chem. Phys. Lett.* 256 (1996) 641–648.
- [17] S. Borowski, T. Kluner, H.J. Freund, I. Klinkmann, K. Al-Shamery, M. Pykavy, V. Staemmler, *Appl. Phys. A* 78 (2004) 223–230.
- [18] M. Pykavy, S. Thiel, T. Kluner, *J. Phys. Chem. B* 106 (2002) 12556.
- [19] S. Borowski, T. Kluner, H.J. Freund, *J. Chem. Phys.* 119 (2003) 10367.
- [20] S.A. Chambers, J.R. Williams, M.A. Henderson, A.G. Joly, M. Varela, S.J. Pennycook, *Surf. Sci.* 587 (2005) L197–L207.
- [21] M.A. Henderson, *Surf. Sci.* 606 (2012) 505–509.
- [22] M.A. Henderson, *Surf. Sci.* 604 (2010) 1800–1807.
- [23] M.A. Henderson, K.M. Rosso, *Surf. Sci.* 605 (2011) 555–563.
- [24] M.A. Henderson, S.A. Chambers, *Surf. Sci.* 449 (2000) 135–150.
- [25] T. Kluner, *Isr. J. Chem.* 45 (2005) 77.
- [26] S. Ohshiro, O. Chiyoda, K. Maekawa, Y. Masui, M. Anpo, H.F. Yamashita, *Comp. R. Chim.* 9 (2006) 846.
- [27] M. Radecka, K. Zakrzewska, M. Wierzbicka, A. Gorzkowska, S. Komornicki, *Solid State Ionics* 157 (2003) 379–386.
- [28] Y.T. Shih, Y.Y. Liao, D.S. Chuu, *Phys. Rev. B* 68 (2003) 075402/1.

- [29] S. Thiel, T. Kluner, M. Wilde, K. Al-Shamery, H.J. Freund, *Chem. Phys.* 228 (1998) 185–203.
- [30] S. Thiel, M. Pykavy, T. Kluner, H.J. Freund, R. Kosloff, V. Staemmler, *Phys. Rev. Lett.* 87 (2001) 077601.
- [31] S. Thiel, M. Pykavy, T. Kluner, H.J. Freund, R. Kosloff, V. Staemmler, *J. Chem. Phys.* 116 (2002) 762–773.
- [32] C.C. Tsai, H.S. Teng, *Appl. Surf. Sci.* 254 (2008) 4912–4918.
- [33] M. Wilde, O. Seiferth, K. Al-Shamery, H.J. Freund, *J. Chem. Phys.* 111 (1999) 1158–1168.
- [34] M. Wilde, I. Beauport, K. Al-Shamery, H.J. Freund, *Surf. Sci.* 390 (1997) 186–193.
- [35] M. Wilde, K. Al-Shamery, H.J. Freund, *SPIE Proc.* 3272 (1998) 152–159.
- [36] M. Yoshida, K. Takanabe, K. Maeda, A. Ishikawa, J. Kubota, Y. Sakata, Y. Ikezawa, K. Domen, *J. Phys. Chem. C* 113 (2009) 10151–10157.
- [37] Y.J. Zhang, Y.C. Wang, W. Yan, T. Li, S. Li, Y.R. Hu, *Appl. Surf. Sci.* 255 (2009) 9508–9511.
- [38] M. Bender, D. Ehrlich, I.N. Yakovkin, F. Rohr, M. Baumer, H. Kuhlénbeck, H.-J. Freund, V. Staemmler, *J. Phys. Condens. Matter* 7 (1995) 5289–5301.
- [39] F. Rohr, M. Baumer, H.-J. Freund, J.A. Mejias, V. Staemmler, S. Muller, L. Hammer, K. Heinz, *Surf. Sci.* 372 (1997) L291.
- [40] V. Maurice, S. Cadot, P. Marcus, *Surf. Sci.* 458 (2000) 195–215.
- [41] C. Xu, M. Hassel, H. Kuhlénbeck, H.-J. Freund, *Surf. Sci.* 258 (1991) 23–24.
- [42] Y. Shiratsuchi, T. Nakatani, S. Kawahara, R. Nakatani, *J. Phys. Conf. Ser.* 165 (2009) 012034.
- [43] K.L. Man, Q. Guo, M.S. Altman, *Surf. Sci.* 600 (2006) 1060–1070.
- [44] D.H. Guo, Q.L. Guo, M.S. Altman, E.G. Wang, *J. Phys. Chem. B* 109 (2005) 20968–20972.
- [45] W. Xiao, K. Xie, Q. Guo, E.G. Wang, *J. Phys. Condens. Matter* 15 (2003) 1155–1163.
- [46] L. Zhang, M. Kuhn, U. Diebold, *J. Vac. Sci. Technol. A* 15 (1997) 1576–1580.
- [47] L. Zhang, M. Kuhn, U. Diebold, *Surf. Sci.* 375 (1997) 1–12.
- [48] A. Pancotti, A. de Siervo, M.F. Carazzolle, R. Landers, G.G. Kleiman, *Top. Catal.* 54 (2011) 90–96.
- [49] P. Borisov, W. Kleemann, *J. Appl. Phys.* 110 (2011) 033917.
- [50] A. Maetaki, K. Kishi, *Surf. Sci.* 411 (1998) 35–45.
- [51] A. Maetaki, M. Yamamoto, H. Matsumoto, K. Kishi, *Suf. Sci.* 445 (2000) 80–88.
- [52] C.P. Huggins, R.M. Nix, *Surf. Sci.* 594 (2005) 163–173.
- [53] W.A.A. Priyantha, G.D. Waddill, *Surf. Sci.* 578 (2005) 149–161.
- [54] Y. Shiratsuchi, T. Nakatani, S. Kawahara, R. Nakatani, *J. Appl. Phys.* 106 (2009) 033903.
- [55] A. Picone, G. Fratesi, M. Riva, G. Bussetti, A. Calloni, A. Brambilla, M.I. Trioni, L. Duo, F. Ciccacci, M. Finazzi, *Phys. Rev. B* 87 (2013) 085403.
- [56] S. Sahoo, T. Mukherjee, K.D. Belashchenko, Ch Binek, *Appl. Phys. Lett.* 91 (2007) 172506.
- [57] X.H. Liu, W. Liu, S. Guo, F. Yang, X.K. Lv, W.J. Gong, Z.D. Zhang, *Appl. Phys. Lett.* 96 (2010) 082501.
- [58] A.M. Venezia, C.M. Loxton, J.A. Horton, *Surf. Sci.* 225 (1990) 195–205.
- [59] N. Shimomura, K. Sawada, T. Nozaki, M. Doi, M. Sahashi, *Appl. Phys. Lett.* 101 (2012) 012403.
- [60] S.A. Chambers, Y. Liang, Y. Gao, *Phys. Rev. B* 61 (2000) 13223.
- [61] T.C. Kaspar, S.E. Chamberlain, M.E. Bowden, R. Colby, V. Shutthanandan, S. Manandhar, Y. Wang, P.V. Sushko, S.A. Chambers, *J. Phys. Condens. Matter* 26 (2014) 135005.
- [62] R. Cheng, B. Xu, C.N. Borca, A. Sokolov, C.-S. Yang, L. Yuan, S.-H. Liou, B. Doudin, P.A. Dowben, *Appl. Phys. Lett.* 79 (2001) 3122–3124.
- [63] J. Dai, J. Tang, H. Xu, L. Spinu, W. Wang, K.-Y. Wang, A. Kumbhar, M. Li, U. Diebold, *Appl. Phys. Lett.* 77 (2000) 2840.
- [64] T.C. Kaspar, S.E. Chamberlain, S.A. Chambers, *Surf. Sci.* 618 (2013) 159–166.
- [65] N. Iwata, T. Kuroda, H. Yamamoto, *Jpn. J. Appl. Phys.* 51 (2012) 11PG12.
- [66] M. Street, W. Echtenkamp, T. Komesu, S. Cao, P.A. Dowben, Ch Binek, *Appl. Phys. Lett.* 104 (2014) 222402.
- [67] Q. Guo, L. Gui, P.J. Möller, K. Binau, *Appl. Surf. Sci.* 92 (1996) 513–518.
- [68] R. Cheng, C.N. Borca, N. Pilet, Bo Xu, L. Yuan, B. Doudin, S.H. Liou, P.A. Dowben, *Appl. Phys. Lett.* 81 (2002) 2109–2111.
- [69] J.A. Wilks, J.A. Kelber, *Appl. Surf. Sci.* 255 (2009) 9543–9547.
- [70] C. Bjelkevig, Z. Mi, J. Xiao, P.A. Dowben, L. Wang, W.-N. Mei, J.A. Kelber, *J. Phys. Condens. Matter* 22 (2010) 302002.
- [71] B. Stypula, J. Stoch, *Corros. Sci.* 36 (1994) 2159–2167.
- [72] B.F. Dzhurinskii, D. Gati, N.P. Sergushin, V.I. Nefedov, Ya V. Salyn, *Russ. J. Inorg. Chem.* 20 (1975) 2307–2314.
- [73] A.R. Brooks, C.R. Clayton, K. Doss, Y.C. Lu, *J. Electrochem. Soc.* 133 (1986) 2459–2464.
- [74] G. Latha, N. Rajendran, S. Rajeswari, *J. Mater. Eng. Perform.* 6 (1997) 743–748.
- [75] A.M. Beccaria, G. Castello, G. Poggi, *Br. Corros. J.* 30 (1995) 283–287.
- [76] J.M. Grimal, P. Marcus, *Corros. Sci.* 33 (1992) 805–814.
- [77] J. Zhang, P.A. Dowben, D. Li, M. Onellion, *Surf. Sci.* 329 (1995) 177–183.
- [78] D. Wooten, I. Ketsman, J. Xiao, Ya B. Losovyj, J. Petrosky, J. McClory, Ya V. Burak, V.T. Adamiv, P.A. Dowben, *Phys. B Condens. Matter* 405 (2010) 461–464.
- [79] J. Wang, J.A. Colón Santana, N. Wu, C. Karunakaran, J. Wang, P.A. Dowben, Ch Binek, *J. Phys. Condens. Matter* 26 (2014) 055012.
- [80] L.E. Davis, N.C. MacDonald, P.W. Palmberg, G.E. Riach, R.E. Weber, *Handbook of Auger Electron Spectroscopy*, second ed., Physical Electronics, Eden Prairie, Minnesota, 1976, pp. 33–77.
- [81] See the NIST XPS Data Base, Available at <http://srdata.nist.gov/XPS> (accessed January 2014).
- [82] S.A. Chambers, T. Droubay, D.R. Jennison, T.R. Davis, *Science* 297 (2002) 827–831.
- [83] C.D. Wagner, *J. Vac. Sci. Technol.* 15 (1978) 518–523.
- [84] C.D. Wagner, D.E. Passoja, H.A. Six, H.F. Hillery, J.A. Taylor, T.G. Kinisky, W.T. Jansen, *J. Vac. Sci. Technol.* 21 (1982) 933–944.
- [85] H.M. Liao, R.N.S. Sodhi, T.W. Coyle, *J. Vac. Sci. Technol. A* 11 (1993) 2681–2686.
- [86] A. Fernandez, A.R. Gonzalez-Elipe, D. Leinen, J.P. Espinos, J.P. Holgado, *Appl. Surf. Sci.* 68 (1993) 453–459.
- [87] T. Nozaki, Y. Sato, T. Ashida, N. Shimomura, M. Sahashi, *Appl. Phys. Express* 7 (2014) 093006.
- [88] W.A. de Heer, C. Berger, X.S. Wu, P.N. First, E.H. Conrad, X.B. Li, T.B. Li, M. Sprinkle, J. Hass, M.L. Sadowski, M. Potemski, G. Martinez, *Solid State Commun.* 143 (1–2) (2007) 92.
- [89] Christian Binek, Peter A. Dowben, Kirill Belashchenko, Jeffrey Kelber, “Magneto-electric voltage controlled spin transistors”, U. S. Patent Application Serial No.: 61766025, filed February 18, 2013, 2013, efileingAck18224783, non-provisional filing number 14182521, February 18, 2014.
- [90] H. Haugen, D. Huertas-Hernando, A. Bratass, *Phys. Rev. B* 77 (2008) 115406.
- [91] C.M. Pradier, F. Rodrigues, P. Marcus, M.V. Landau, M.L. Kaliya, A. Gutman, M. Herskowitz, *Appl. Catal. B Env.* 27 (2000) 73–85.
- [92] A. Atrens, A.S. Lim, *Appl. Phys. A* 51 (1990) 411–418.
- [93] A. Lebugle, U. Axelsson, R. Nyholm, N. Martensson, *Phys. Scr.* 23 (1981) 825–827.
- [94] B. Brox, I. Olefjord, U. Jelvestam, *J. Electrochem. Soc.* 132 (1985) 2854–2861.
- [95] C. Schmidt, H. Oetzmann, P. Hess, R. Nowak, *Appl. Surf. Sci.* 43 (1989) 11–16.
- [96] A. Sokolov, C.-S. Yang, L. Yuan, S.-H. Liou, R. Cheng, H.-K. Jeong, T. Komesu, B. Xu, C.N. Borca, P.A. Dowben, B. Doudin, *Europhys. Lett.* 58 (2002) 448–454.
- [97] A. Sokolov, C.-S. Yang, L. Yuan, S.-H. Liou, Ruihua Cheng, B. Xu, C.N. Borca, P.A. Dowben, B. Doudin, *J. Appl. Phys.* 91 (2002) 8801–8803.
- [98] P.A. Dowben, B. Doudin, in: M. Donath, W. Nolting (Eds.), *Local Moment Ferromagnets: Unique Properties for Modern Applications*, Lecture Notes in Physics, vol. 678, Springer, 2005, pp. 309–326. ISBN 0075-8450.
- [99] Q. Chen, M. Onellion, A. Wall, P.A. Dowben, *J. Phys. Condens. Matter* 4 (1992) 7985–7996.
- [100] C.A.F. Vaz, J.A.C. Bland, G. Lauhoff, *Repts. Prog. Phys.* 71 (2008) 056501.